PHYSICAL REVIEW B VOLUME 44, NUMBER 22 1 DECEMBER 1991-II

Scaling relations for interface motion through disordered media: Application to two-dimensional fluid invasion

Nicos Martys* and Mark O. Robbins
Department of Physics and Astronomy, Johns Hopkins University, Baltimore, Maryland 21218

Marek Cieplak
Institute of Physics, Polish Academy of Sciences, 02-668 Warsaw, Poland
(Received 29 July 1991)

We consider the critical transitions that occur as the force driving an interface through a random medium is increased. The total displacement of the interface, and the incremental advance after a small increase in force, diverge as the force approaches a critical depinning threshold. At the critical force there is a power-law distribution of growth sizes. General scaling relations are derived between the critical exponents associated with such transitions. These scaling relations are tested on a model system — fluid invasion of a two-dimensional porous medium. Critical exponents are determined from simulations using finite-size-scaling techniques. Two universality classes are identified: percolation and depinning. In both cases the calculated exponents obey the scaling relations.

I. INTRODUCTION

Two areas of great recent activity have been the study of patterns formed by moving interfaces[1–3] and of critical phenomena that occur at the onset of steady-state motion.[4–10] Models of interface motion describe growth phenomena; including aggregation, deposition, crystallization, magnetic-domain-wall motion, spreading, and fluid invasion.[1–3] Nonlinearities and randomness in these growth processes lead to a rich variety of fractal growth morphologies. Critical transitions occur at the onset of motion in charge-density-wave (CDW) conductors,[4] flux lattices,[5] fluid interfaces,[6–8] magnetic domain walls,[9] model sandpiles,[10] and earthquake faults.[11] Unlike normal critical phenomena, no fine tuning of a parameter is necessary to place these systems near their critical point — one need only drive them at a low rate. As discussed by Bak and co-workers,[10] many natural systems may be in such "self-organized critical" (SOC) states.

In this paper we consider a class of models which combines these two fields of interest: motion of an interface driven by a force through a disordered medium. The interface may separate magnetic domains with different spin orientations or two different fluids or solids. The driving force may be thermodynamic, as in the coarsening of supercooled magnetic or fluid domains. It may also be external. In the case of fluid invasion, the external force is the pressure driving the invading fluid into the region of a porous medium which is occupied by the displaced fluid. In magnetic systems, it would correspond to an external field favoring one spin orientation over another.

The idea that the onset of motion in a disordered system could be a critical transition was first advanced by Fisher[4] in the context of CDW conductors. The basic argument is readily extended to many other cases, including interfaces. If the spatial dimension is sufficiently low, the interface will be distorted by the disorder until it reaches a local energy minimum. At zero applied force there will be a rich hierarchy of metastable states. The interface will initially be "pinned" in one local minimum. As the force increases, that minimum may become unstable, allowing the interface to advance to the nearest metastable state. The number of metastable states decreases with increasing force so that larger rearrangements of the interface are needed to reach a new metastable state. It is natural to associate the scale of rearrangements with a diverging coherence length. At a critical depinning force, the last state becomes unstable and the entire system evolves coherently.

In the following sections we identify a number of critical quantities which describe the onset of interface motion as the critical force is approached from below. These include the total advance of the interface, the incremental advance after a small increase in force, and the distribution of incremental growths at the critical force. We then develop general scaling relations between the associated critical exponents. These results are applied to a specific model system — fluid invasion of two-dimensional (2D) porous media. Finite-size scaling techniques are used to find the critical exponents for this system. Two universality classes are identified, percolation and depinning. The exponents for both classes satisfy our scaling relations. Before presenting these results we briefly review related work.

Substantial progress has been made in describing the critical dynamics of CDW conductors. In contrast to driven interfaces, the CDW is always affected by all impurities. Both the CDW order parameter and the disorder are defined throughout the conductor. This leads to a unique dynamic state above the depinning transition. Simulations and general arguments indicate that

 ©1991 The American Physical Society

this state must be periodic.[12,13] Values for the critical exponents have been derived in mean-field theory[4] and through simulations.[12–14] Measurements confirm that depinning is a critical phenomenon,[15,16] and in some cases give exponents which agree with simulations.[12,16] However, thermal excitations and variations in CDW amplitude appear to complicate the behavior in other cases.[15,17]

A driven interface interacts with a lower dimensional subset of the disordered system at each instant. This subset changes as the interface advances, and there can be no periodic state at the onset of flow. There are several different classes of moving interfaces, depending on the dimensions of the interface and of the disordered region. In magnetic domain wall motion[18,19] and fluid invasion[3,6,7] or segregation,[20] the interface is initially $d-1$ dimensional and moves through a system with disorder in all d dimensions. In spreading,[8] the disorder is confined to the $d-1=2$ dimensional substrate and the fluid interface only intersects the disordered medium along the one-dimensional "contact line." The problem can be reduced to motion of the 1D contact line over the 2D substrate. However, the elastic spectrum of the contact line is affected by deformations of the interface away from the contact line.[21] This may lead to a new universality class. Other interesting possibilities include pinning of dislocation lines or individual vortices where a $(d-2)$-dimensional object moves through a d-dimensional disordered system.

Bruinsma and Aeppli[18] and Koplik and Levine[19] have independently considered a continuum model of a driven magnetic domain wall. The interface was represented by a single-valued function, $f(\mathbf{x})$, giving the height above a point $\mathbf{x}$ in the reference plane. The equation of motion is

$$\frac{df}{dt} = F + \Gamma\nabla^2 f + g\,\eta(\mathbf{x},t), \tag{1}$$

where F is the applied force, Γ is an effective elastic constant, η is a random field with δ-function correlations in space or time, and g characterizes the effective strength of the disorder. Koplik and Levine noted that this equation might also describe fluid invasion with the two-spin domains corresponding to the invading and displaced fluids. This analogy is discussed further below.

Bruinsma and Aeppli used a scaling approach to study Eq. (1). They concluded that disorder could pin the interface for $d<5$. Koplik and Levine[19] applied mean-field theory, perturbation techniques, and numerical integration and reached different conclusions. In particular, they found no pinning for $d>3$. They also found different scaling for the interface width and for the force needed to initiate motion in lower dimensions. Neither of these papers considered the possibility of a critical transition at the onset of interface motion.

Equations of motion very similar to Eq. (1) have been used in modeling growth. One of the most widely studied[22–25] is that of Kardar, Parisi, and Zhang (KPZ).[22] Their equation has an additional term proportional to $|\nabla f|^2$ which represents a correction for lateral growth. In addition, the disorder is annealed rather than quenched – it is a random function of time rather than of position. For annealed disorder there is no pinning and thus no critical transition. The average force on the interface is unimportant and may be removed from the equations.

There are several ways in which Eq. (1) and the KPZ equation provide an incomplete description of fluid invasion or magnetic domain wall motion. The first is that the interface shape is approximated by a single-valued function. Experiments show that the interfaces are not single valued.[3,26–31] A related problem is that growth is directed along a fixed vertical axis rather than along the local surface normal. Finally, it is unclear whether continuum models produce the same dynamics as that for discrete spins or pores.[23,32] Indeed, Koplik and Levine found an ultraviolet singularity in their model. Similar divergences occur in CDW's and fluid spreading.[4,8]

The most widely studied model of fluid invasion, percolation (IP),[3,33] overcomes these deficiencies. The pore space is divided into larger regions called "pores" and smaller "throats" which connect them. Segments of the interface in each throat or pore are *assumed to be independent.* If the invading fluid is nonwetting, a higher capillary pressure is needed to penetrate narrower throats. At a given pressure, some fraction of the throats will be invadable, and the remainder will not. The statistics of invadable throats is analogous to that of connected bonds in bond percolation models.[34] At a critical pressure P_c, the fraction of invadable bonds reaches the percolation probability and there is a connected path of passable throats spanning the system. No further displacement will occur because there is a continuous path of the invading fluid. It was argued that the same picture should describe wetting invasion, with the pores replacing throats as the barriers to interface motion.[35]

The fractal patterns with pore scale fingers predicted by the IP model have been observed in many experiments on nonwetting invasion.[3,26] However, studies of wetting invasion show coherent growth.[27–31] The first indication of when and why the IP model breaks down came from experiments on square network models of porous media by Lenormand and co-workers.[26,27] They showed that invasion by perfectly nonwetting fluids was consistent with the IP model — each throat was invaded independently. However, invasion by wetting fluids occurred through different mechanisms, and invasion of neighboring pores was not independent. The correlations tended to smooth the interface, and the pattern did not appear fractal.[27]

Recently, we have completed detailed studies of the changes in the invaded pattern with the wetting properties of the invading fluid.[6,36] The latter are described by the contact angle θ at which a static fluid interface intersects the solid.[37] By convention, the invading fluid is loosely called nonwetting when θ is near 180° and wetting when θ is near 0°. The generic phase diagram for this system is illustrated in Fig. 1. For each θ there is a critical pressure P_c at which the invading fluid will first span an infinite system. There is a critical contact angle, θ_c, which depends on the geometry of the pore space. For $\theta > \theta_c$ (invading fluid less wetting), there is a percolation transition with increasing P and the in-

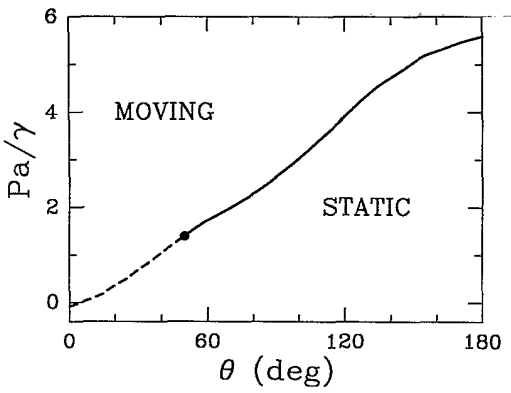

FIG. 1. Typical (θ, P) phase diagram for quasistatic invasion. Solid (dashed) lines indicate P_c for percolation (depinning). A solid circle indicates θ_c. Results are symmetric for $P \longleftrightarrow -P$ and $\theta \longleftrightarrow 180 - \theta$ which corresponds to reversing both flow direction and fluids.

vaded pattern is a self-similar fractal. Invasion for $\theta < \theta_c$ is completely different. The invaded region is compact, and its boundary is a self-affine fractal. The calculated roughness exponent,[6] $H = 0.81$, is consistent with recent experiments on wetting invasion.[30,31] The change in morphology for $\theta < \theta_c$ is related to the presence of an effective macroscopic surface tension which controls the motion of curved sections of the interface.[6] An analogous quantity had been assumed in theories of viscous fingerwidths in porous media[28,29,38,39] and by Koplik and Levine [Eq. (1)].[40] However, there had been no microscopic theory for its origin in wetting invasion, or for its absence in nonwetting invasion.

The above studies also revealed divergences in the total and incremental invaded volumes[41] as P was increased to P_c. The behavior in wetting and nonwetting invasion was markedly different, but it was not possible to obtain accurate critical exponents from data for a single system size. This lead us to develop the finite-size scaling approach which is one main focus of this paper.

The outline of the paper is as follows. Section II describes the model porous media used, the growth algorithm, and the critical quantities and exponents. The following section contains derivations of general scaling relations for interface motion. In Sec. IV finite-size scaling techniques are used to determine critical exponents for invasion percolation and depinning. In both cases, the exponents satisfy the scaling relations. The final section presents a summary and conclusions.

II. APPLICATION TO 2D FLUID INVASION

Simple model 2D porous media were constructed[36] by placing disks of random radii r on a triangular lattice with lattice constant a. Results below are for a highly disordered system with r/a uniformly distributed between 0.05 and 0.49. The critical angle for this system is $\theta_c \approx 49°$, and the phase diagram is shown in Fig. 1. Other systems studied in Ref. 36 showed similar behavior. The only exception is that a direct transition from percolation to *faceted* growth was observed in samples with little disorder (small range of radii). This transition is closely related to that found in recent work on magnetic systems.[9]

Since we are interested in the quasistatic advance of the interface at pressures below P_c, viscous pressure drops may be neglected. The advance of the interface is controlled by the capillary pressure $P = \gamma\kappa$, where γ is the surface tension and κ the curvature of the interface. We model quasistatic invasion as a stepwise process where each unstable section of the interface moves to the next stable or nearly stable configuration in turn. The growth algorithm is briefly outlined below and described in detail in Ref. 36.

A fixed pressure drop P is applied across the interface, which consists of a sequence of circular arcs connecting pairs of disks (Fig. 2). Stable arcs must have radius γ/P and intersect the disks at θ. Three types of instability are identified: "burst" — no arc with radius γ/P intersects both disks at θ, "touch" — an arc connecting two disks intersects a third, and "overlap"—arcs between successive pairs of disks intersect. As θ decreases, the dominant instability changes from bursts to overlaps. Bursts and touches are local mechanisms which can be included in percolation models.[3,33] In contrast, overlap depends on the configuration of adjacent arcs. As can be seen from Fig. 2, overlap becomes more likely as the bond angle α between successive disks decreases. Sharp bends in the interface are likely to become unstable due to overlaps. Thus overlaps smooth the interface and lead to cooperative motion.

For the results described below, growth was initiated from a flat interface at the bottom of the system. We checked that there was no anisotropy by growing from interfaces with inequivalent orientations, and also checked that starting from a self-affine interface (a one-dimensional random walk[3]) gave the same statistics.

The pressure was adjusted so that a single segment of the initial interface became unstable. This segment of

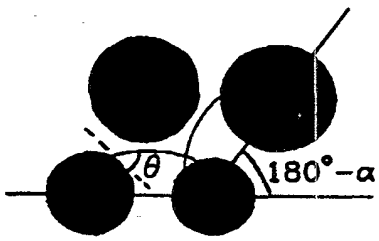

FIG. 2. Arcs between successive disks on an interface are shown. The invading fluid is below the interface and θ and α are measured as indicated. For this case $\alpha = 120°$. Decreasing α or θ increases the probability of overlaps. A touch instability would occur if one of the arcs intersected the upper left disk before overlapping with the other arc.

the interface was advanced. Any resulting instabilities were advanced in turn until a new stable interface was reached. The value of P was then increased again until a single segment of the new interface became unstable, and the process was repeated until the system was filled. The pressure at which the interface first spanned the system was calculated for each realization of the random medium. In the limit $L \to \infty$ this pressure approaches the critical pressure P_c.

Growth was characterized by the total invaded volume V_t, the total external[42] interfacial area S_e, and the volume and shape of regions invaded after each increment in P. Figure 3 shows examples of these individual growths at (a) $\theta = 25°$ and (b) $\theta = 90°$, which are below and above θ_c, respectively. In each case, the lower interface was stable at a pressure about 1% below P_c. The black region shows the volume V invaded after a single segment of the interface became unstable. Note the dramatic change with θ in the structure of invaded regions. For small θ, an entire segment of the interface advances coherently. At large θ, each segment of the interface advances independently forming a fractal pattern characteristic of percolation. In many places the invading fluid completely surrounds regions of the displaced fluid. Such "trapped" regions were not allowed to shrink further, since the displaced fluid is assumed to be incompressible.[33,35]

At any θ, the entire system must be spanned by the invaded pattern at P_c. We find a power-law divergence of V_t as $P \to P_c$:

$$V_t \propto (P_c - P)^{-\psi}. \tag{2}$$

There is a related divergence in the mean volume of individual growths:

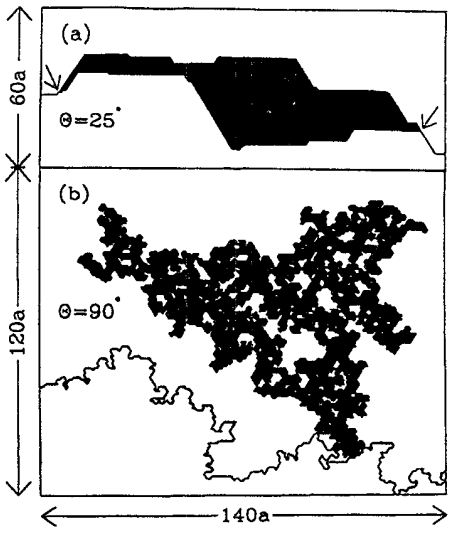

FIG. 3. Volume V invaded (black) when a single arc became unstable at the indicated θ and $(P_c - P)/P_c \sim 0.01$. The length λ is the Cartesian width of the advancing interface segment [distance between arrows in (a)]. Both plots show sections of $L = 1000$ systems.

$$\langle V \rangle \propto (P_c - P)^{-\phi}, \tag{3}$$

where the angular brackets denote an average over growths in a range of pressures about P. For fractal growth the external interfacial area also diverges:

$$S_e \propto (P_c - P)^{-\omega}. \tag{4}$$

For compact growth S_e remains of order the system size.

A measure of the degree of coherence, λ, was defined as the Cartesian width of the continuous segment of the interface around the initial instability which advanced [Fig. 3(a)]. For $\theta > \theta_c$, λ saturates at a characteristic fingerwidth as $P \to P_c$: Beyond this scale growth is uncorrelated. As θ decreases to θ_c, the fingerwidth diverges.[36] For all $\theta < \theta_c$ the value of λ diverges at P_c — as expected for a depinning transition, the entire interface advances coherently.[6] We show below that

$$\langle \lambda^d \rangle \propto (P_c - P)^{-\phi}, \tag{5}$$

where d is the Euclidean dimension.

The divergences of V_t, S_e, $< V >$, and $< \lambda >$ are cut off in systems of finite size. In the following section we describe a finite-size scaling ansatz that allows us to determine critical exponents from collapses of results for different L onto universal curves.

III. FINITE-SIZE SCALING ANSATZ AND SCALING RELATIONS

A. Divergences as $P \to P_c$

In the last section we identified several lengths, areas, and volumes that characterize the growth of the invaded pattern. While they are expected to diverge at P_c in an infinite system, their values must saturate at some power of the system size in a finite system. Figure 4 shows an example of this saturation for $\langle V \rangle$ at $\theta = 25°$. Results for the largest system sizes follow the asymptotic power-law divergence until typical growths are of order L^2. Then they begin to fall below the asymptotic curve. All results for the smallest system, $L = 30$, are affected by finite size. The saturation illustrated in Fig. 4 makes it difficult to determine the critical pressure and exponents accurately. In this section we introduce a finite-size scaling ansatz to overcome this difficulty, and derive a set of scaling laws between critical exponents. These relations are summarized in Table I.

Our approach closely follows techniques used for equilibrium critical phenomena and for other critical phenomena such as percolation.[34] The central idea is that the only relevant length scales in the critical region near P_c are the system size and a single[43] correlation length ξ, which diverges as

$$\xi \propto |P_c - P|^{-\nu}. \tag{6}$$

Thus, appropriately normalized quantities should only depend on the ratio of L to ξ. This ratio is usually expressed[34] in terms of a scaling parameter

$$x \equiv L^{1/\nu}(P - P_c)/P_c \tag{7}$$

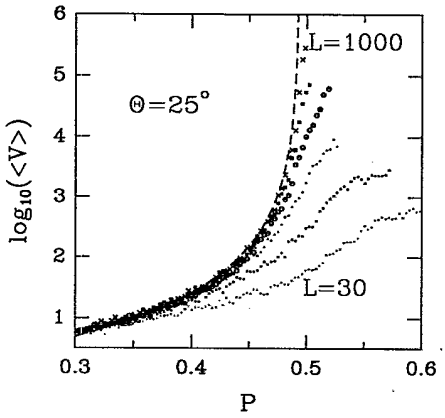

FIG. 4. Plot of $\langle V\rangle$ vs P for $\theta = 25°$, showing the finite-size saturation at different system sizes. In order of increasing height, L=30, 60, 120, 240, 480, and 1000. The dashed line shows the power-law divergence for an infinite system.

so that functions are analytic in P.

We begin by considering the form of the equation which relates the total volume invaded to the pressure and system size. At P_c the invaded region will span the system. The volume should then scale as L^{D_f}, where D_f is the fractal dimension characterizing the invaded region. For nonwetting invasion this is the fractal dimension of invasion percolation.[35,36,44] For wetting invasion, growth is compact[6] and D_f must equal the Euclidean dimension d. The expected scaling of the mean invaded volume with L at P_c will automatically be satisfied if

$$V_t(P,L) = L^{D_f} g(L^{1/\nu}(P-P_c)/P_c), \tag{8}$$

where g is a universal function whose argument vanishes at P_c.

The asymptotic form of g can be determined from simple arguments. For $L^{1/\nu}(P-P_c)/P_c \ll -1$ the characteristic scale of forward growths should be of order ξ, which is much less than L. If growth is started from a $d-1$ dimensional boundary of the system,[45] the total invaded volume at small P will scale with the boundary's area, L^{d-1}. This scaling requires $g(x) \sim |x|^{-\nu(D_f-d+1)}$ at large negative x. Substituting this expression into Eq. (8), we find $V_t \propto L^{d-1}(P_c-P)^{-\nu(D_f+1-d)}$. This equation and Eq. (2) provide our first scaling relation (Table I): $\psi = \nu(D_f+1-d)$. The physical meaning of our result for V_t is made clear by reexpressing it in terms of ξ: $V_t \propto (L/\xi)^{d-1}\xi^{D_f}$. Thus for fractal growth, V_t is the sum of $(L/\xi)^{d-1}$ independent growths with size of order ξ^{D_f}. For compact growth ($D_f = d$), $V_t \propto L\xi$ and $\psi = \nu$. In either case, ξ is a measure of the total forward advance of the interface. Not surprisingly, finite-size effects enter when the interface has advanced by a distance comparable to the system size.

Analogous arguments can be used to determine the scaling of the total surface area S_e of the external interface of the invaded region:[42]

$$S_e(P,L) = L^{D_e} g_S(L^{1/\nu}(P-P_c)/P_c), \tag{9}$$

where D_e is the fractal dimension of the external interface. As above, the asymptotic form of g_S for $L^{1/\nu}(P-P_c)/P_c \ll -1$ can be determined by noting that S_e must scale with L^{d-1} in this regime. This requires $g_S(x) \propto |x|^{-\nu(D_e+1-d)}$. In conjunction with Eq. (4) we find a second scaling relation, $\omega = \nu(D_e+1-d)$. For fractal growth at low pressures, $S_e \propto (L/\xi)^{d-1}\xi^{D_e}$ — the sum of contributions from $(L/\xi)^{d-1}$ independent growths with scale ξ. For compact growth with a faceted or self-affine interface, $D_e = d-1$. Thus g_S is constant and $S_e \propto L^{d-1}$.

We next define a susceptibility $\chi \equiv L^{1-d}dV_t/dP$, the growth in response to a small change in pressure normalized by the size of the boundary. Differentiating Eq. (8) we find

$$\chi(P,L) = L^{B_\chi} f(L^{1/\nu}(P-P_c)/P_c), \tag{10}$$

where the exponent $B_\chi = D_f + 1 - d + 1/\nu$ and $f(x) = P_c^{-1}dg/dx$. From the form of g in the limit $L^{1/\nu}(P-P_c)/P_c \ll -1$, one finds $f(x) \sim |x|^{-\nu B_\chi}$. This guarantees that χ is independent of system size, and implies that in the limit $L \to \infty$

$$\chi(P) \sim (P_c - P)^{-\phi_\chi}, \tag{11}$$

with $\phi_\chi = \nu B_\chi$.

We now have a relation between the exponents characterizing the divergences of the total volume and susceptibility. However, in our simulations we are concerned with the scaling properties of the mean size of individual growths $\langle V\rangle$. This quantity can be related to χ in the following way. First note that

$$L^{d-1}\chi(P,L) = \frac{dV_t}{dP} \approx \Delta V/\Delta P = N\langle V\rangle/\Delta P, \tag{12}$$

where N is the number of growths in a pressure range $[P-\Delta P/2, P+\Delta P/2]$. This number can be written as $N = S_e \Delta P(dy/dP)$, where $\Delta P(dy/dP)$ is the change in the fraction y of stable interface segments.[46] Near P_c, dy/dP is approximately constant and we may write

TABLE I. General scaling laws obeyed by critical exponents for invasion and specialized forms for compact growth where $D_f = d$ and $D_e = d-1$.

General	Compact growth
$\psi = \nu(D_f+1-d)$	$\psi = \nu$
$\omega = \nu(D_e+1-d)$	$\omega = 0$
$\phi = \nu B = \nu(D_f - D_e)+1$	$\phi = 1+\nu$
$\phi_\chi = \nu B_\chi = \nu(D_f+1-d)+1$	$\phi_\chi = 1+\nu$
$B = D_f + 1/\nu - D_e$	$B = 1+1/\nu$
$B_\chi = B + D_e + 1 - d$	$B_\chi = B$
$\tilde{B} \le Bd/D_f$	$\tilde{B} = B$
$\tau' D_f = D_f + D_e - 1/\nu$	$\tau' d = 2d - 1 - 1/\nu$

$$\langle V\rangle = \frac{\Delta P}{N}\frac{dV_t}{dP} = \frac{1}{S_e}\frac{dV_t}{dP}\frac{dP}{dy} \propto \chi\frac{L^{d-1}}{S_e}. \tag{13}$$

From Eq. (13) we see that $\langle V\rangle$ behaves like a different type of susceptibility. It is proportional to the response to a small change in pressure *per unit interfacial area.*

Combining our scaling expressions for χ and S_e we find

$$\langle V\rangle \propto L^B h(L^{1/\nu}(P-P_c)/P_c)\ , \tag{14}$$

where $B = D_f - D_e + 1/\nu$ and $h(x) = f(x)/g_S(x)$. When $L^{1/\nu}(P-P_c)/P_c \ll -1$ we should find that $\langle V\rangle \propto (P_c - P)^{-\phi}$ and is independent of L. The latter requires $h(x) \propto |x|^{-B\nu}$ which is consistent with the asymptotic forms for f and g_S. Inserting this form into Eq. (14) we find $\langle V\rangle \propto (P_c - P)^{-B\nu}$. With Eq. (3) this expression implies a scaling relation for ϕ, $\phi = B\nu = \nu(D_f - D_e)+1$. For compact growth (wetting invasion), $D_f - D_e = 1$ so that $\phi = 1+\nu$.

As noted above, the entire system advances coherently at P_c when growth is compact. The coherence length λ is a measure of the extent of growth *along* the interface (Fig. 3). If all dimensions of growths diverge with the same exponent, one expects that $\langle\lambda^d\rangle \propto \langle V\rangle \propto (P_c - P)^{-\phi}$ in the critical regime. Results for wetting invasion show that $\langle\lambda^d\rangle$ and $\langle V\rangle$ do indeed track each other until they become comparable to the system size.[47] Given this proportionality, the two quantities must have the same finite-size scaling form, implying[48]

$$\langle\lambda^d\rangle = L^B h_\lambda(L^{1/\nu}(P-P_c)/P_c). \tag{15}$$

The universal function h_λ will not in general be the same as h. However, it must have the same asymptotic behavior for $L^{1/\nu}(P-P_c)/P_c \ll -1$.

One can define analogous scaling relations for other lengths which characterize individual growths such as the radius of gyration, or the total width or height. We will consider only one of these additional lengths, $\bar\lambda$, which is the maximum Cartesian distance between points on the initial interface which advance in a single growth. This length differs from λ because the growth need not be contiguous. For example, a fractal growth like that illustrated in Fig. 3 may wander back into contact with the original interface. This gives a large $\bar\lambda$, but λ is small because the interface did not advance coherently. We find that $\bar\lambda$ diverges for both percolation and compact growth, and that

$$\langle\bar\lambda^d\rangle = L^{\bar B} h_{\bar\lambda}(L^{1/\nu}(P-P_c)/P_c). \tag{16}$$

In compact growth, $\bar B = B$ and $\bar\lambda \propto \lambda$. For self-similar growth, $\bar\lambda$ is bounded by the characteristic radius of gyration of the growths. From the definition of fractal scaling, $R_g \propto V^{1/D_f}$ for individual growths. If $\langle\bar\lambda^d\rangle \propto \langle R_g^d\rangle$ then $\bar B = Bd/D_f$. In general, this is an upper bound for $\bar B$, but we find the equality holds for the system discussed in the next section. Note that it holds in any case for compact growth.

B. Distribution of growths at P_c

The divergence of quantities such as $\langle\lambda^d\rangle$ and $\langle V\rangle$ at P_c is typically associated with a power-law distribution of events in an infinite system. For example, the probability $\rho(V)$ of a growth of size V should scale as[49] $\rho(V) \propto V^{-\tau'}$. Such distributions are truncated in finite systems, and we now consider finite-size scaling forms for them.

The distribution of growth volumes V in a system of size L will be cut off at $\sim L^{D_f}$. For growths much larger than a lattice constant, the shape of the distribution should only depend on the ratio of V to this cutoff. We will show below that $\tau' > 1$. In this case, the normalization of ρ is dominated by small growths, and $\rho(V,L)$ is independent of L for $V \ll L^{D_f}$. Thus[25]

$$\rho(V,L) = L^{-\tau' D_f} p_V(V/L^{D_f}), \tag{17}$$

where p_V is a universal scaling function for the distribution of growths and the power of L multiplying p_V is determined by requiring that $\rho(V) \propto L^0 V^{-\tau'}$ for $V \ll L^{D_f}$.

The exponent τ' can be directly related to the exponents describing the divergence of $\langle V\rangle$ as $P \to P_c$. Equation (17) implies that for $P = P_c$

$$\begin{aligned}\langle V\rangle &= \int dV\, V\rho(V/L^{D_f}) \\ &= L^{D_f(2-\tau')}\int dy\, y\, p_V(y),\end{aligned} \tag{18}$$

where $y = V/L^{D_f}$. The scaling of $\langle V\rangle$ with L at P_c is also given by Eq. (14): $\langle V\rangle \sim L^B$. Equating exponents we obtain

$$D_f(2-\tau') = B = D_f - D_e + \nu^{-1} \tag{19}$$

or

$$\tau' D_f = D_f + D_e - \nu^{-1}. \tag{20}$$

For compact growth, $\tau' d = (2d - 1 - \nu^{-1})$.

Equation (20) can be obtained in an alternative way, where we use the distribution function $\rho(V)$ for an infinite system. In this case there must be a cutoff in ρ for $P < P_c$ due to the finite correlation length ξ. The exact form of the cutoff is unimportant and we use the common assumption[34]

$$\rho(V) \propto V^{-\tau'}\exp(-V/\xi^{D_f}). \tag{21}$$

Then we have

$$\langle V\rangle \propto \int dV\, V V^{-\tau'}\exp(-V/\xi^{D_f}) \tag{22}$$

$$\propto \xi^{D_f(2-\tau')}\int dy\, y^{1-\tau'}\exp(-y) \tag{23}$$

$$\propto (P_c - P)^{-D_f\nu(2-\tau')}. \tag{24}$$

From Eq. (3) we must have $\phi = D_f\nu(2-\tau')$. Since $\phi = B\nu$, we have $B = D_f(2-\tau')$ as found above.

In the depinning regime (compact growth) we are interested in comparing lateral and forward growths. Hence we also study the distribution of λ^d. By the same arguments we must have

$$\rho(\lambda^d, L) = L^{\tau' d} p_\lambda(\lambda^d / L^d). \quad (25)$$

with $\rho(\lambda^d) \sim (\lambda^d)^{-\tau'}$ when $\lambda \ll L$. In principle, the exponent τ' could be different for V and λ^d. However, we have noted above that $\langle V \rangle$ and $\langle \lambda^d \rangle$ diverge with the same exponent ϕ. This combined with the scaling relation between τ' and ϕ guarantees that the distributions have the same value of τ' in the system studied here.

The scaling relations derived in this section are summarized in Table I. Note that at most three exponents are needed to determine all others. These are most naturally chosen as ν and the bulk and surface fractal dimensions. The latter are known for many growth processes, including percolation and compact growth ($D_f = D_e + 1 = d$). In such cases ν is the only unknown exponent. We now apply these scaling relations to wetting and nonwetting invasion of 2D porous media.

IV. FINITE-SIZE SCALING RESULTS FOR 2D FLUID INVASION

In order to contrast wetting and nonwetting invasion, we primarily examined growth for $\theta = 25°$ and 179° which are far below and above θ_c, respectively. These cases were compared to $\theta = 40°$ and 90° to test for universality. For simulations at $\theta = 25°$ and 40° the system's dimensions[50] were La wide by $\sqrt{3}La$ high, with $L = 30, 60, 120, 240, 480$, and 1000. At $\theta = 90°$ and 179°, the dimensions were $La \times La$ with $L = 30, 60, 120, 300$, and 600.

In the following sections, all lengths are expressed in units of the lattice constant a, which is taken to be unity. Pressures are quoted in units of γ/a. Values of P_c and all critical exponents are given in Table II. There and below, error bars give the maximum range which is consistent with the data. They do not include any estimate of systematic errors.

A. Total volume invaded

A simultaneous fit of all scaling parameters is rather complicated. Thus we began by finding values for P_c and D_f, using the fact that V_t/L^{D_f} is independent of system size at P_c [Eq. (8)]. The value of ν was then found by collapsing data for all P and L. We describe this procedure for wetting invasion, and then quote the results found in the same way for nonwetting invasion.

For the compact growth found in wetting invasion, D_f should be equal to 2. Figure 5 shows V_t/L^2 versus P for $\theta = 25°$. Note that the curves cross at the same pressure, which thus corresponds to P_c. Values of D_f below 1.95 gave noticeably poorer crossing of these curves, and values of $D_f > 2$ are of course unphysical. From the intersection of the curves with $D_f = 2$ we conclude that $P_c = 0.4935 \pm 0.0005$.

Enlargement of Fig. 5 reveals that results for the two smallest systems (L=30 and 60) lie slightly below the intersection of the other curves. Corrections to finite-size scaling are needed to fit data for these small systems. As seen in Fig. 4, results for L=30 and 60 begin to deviate from the infinite system behavior at very low pressures.

TABLE II. Critical exponents from finite-size scaling fits for wetting and nonwetting invasion. All values were determined independently except B_χ which was calculated from Table I. The value of D_e was obtained from direct analysis of invaded patterns. Error bars indicate the maximum range consistent with our data. Within these uncertainties, all exponents are consistent with the scaling laws of Table I. Exact values for ordinary 2D percolation (Ref. 34) are also given, with ψ, ϕ, B, and τ' calculated from Table I. Within our accuracy, exponents for nonwetting invasion equal those for 2D percolation (Ref. 49).

Exponent	Wetting invasion $\theta = 25°$ $P_c = 0.4935 \pm 0.0005$	Nonwetting invasion $\theta = 179°$ $P_c = 5.62 \pm 0.02$	Percolation
D_f	2	1.88 ± 0.04	$\frac{91}{48} \approx 1.90$
D_e	1	1.32 ± 0.02	$\frac{4}{3} \approx 1.33$
ν	1.30 ± 0.05	1.32 ± 0.07	$\frac{4}{3} \approx 1.33$
B	1.75 ± 0.10	1.30 ± 0.10	$\frac{21}{16} \approx 1.31$
$\bar{B}$	1.75 ± 0.10	1.3 ± 0.1	$\frac{18}{13} \approx 1.38$
B_χ	1.75 ± 0.10	1.62 ± 0.10	$\frac{79}{48} \approx 1.65$
ψ	1.30 ± 0.05	1.16 ± 0.10	$\frac{43}{36} \approx 1.19$
ϕ	2.30 ± 0.05	1.72 ± 0.20	$\frac{16}{9} \approx 1.78$
ω	0	0.42 ± 0.05	$\frac{4}{9} \approx 0.44$
τ'	1.125 ± 0.025	1.30 ± 0.05	$\frac{17}{13} \approx 1.31$

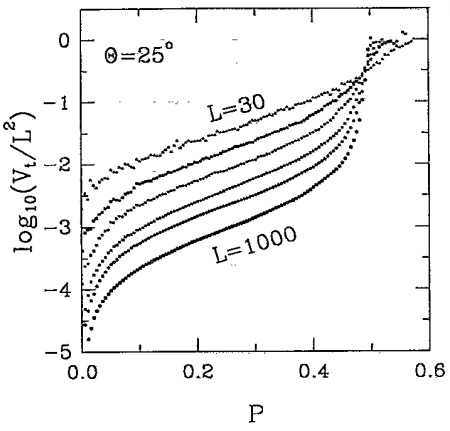

FIG. 5. Plot of $\log_{10}(V_t/L^2)$ vs P at $\theta = 25°$ for $L = 30, 60, 120, 240, 480$, and 1000, in order of decreasing height. Ideally, all curves should intersect at $P = P_c$.

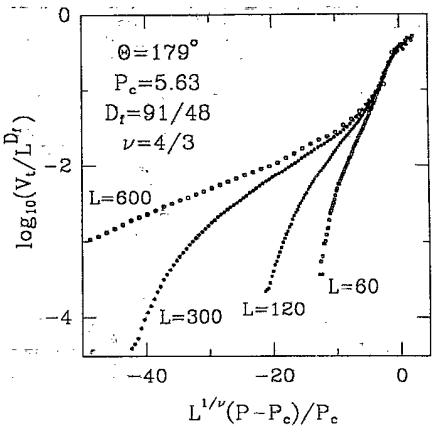

FIG. 7. Plot of $\log_{10}(V_t/L^{D_f})$ vs $L^{1/\nu}(P-P_c)/P_c$ for $\theta = 179°$ (nonwetting regime) with L ranging from 60 to 600.

We will see below that the discreteness of the lattice is important at these pressures ($P < 0.4$). For this reason, only data from the four largest system sizes (L= 120 to 1000) will be used to determine critical exponents.

With reasonable values of P_c and D_f in hand, the only remaining free parameter is ν. In Fig. 6 we show V_t/L^2 versus $x = L^{1/\nu}(P - P_c)/P_c$, where the value of $\nu = 1.3$ has been chosen to collapse all results onto a single universal curve [Eq. (8)] at small values of the scaling parameter x. Depending on the value of P_c (0.4935 ± 0.0005), the best fit for ν ranged from 1.25 to 1.35.

Note that the curves associated with different system sizes do not overlap at early stages of growth [large negative $L^{1/\nu}(P - P_c)/P_c$]. At these smaller pressures the total forward motion of the interface is of order a lattice spacing ($L^{-1}V_t \sim 1$). The finite-size-scaling ansatz does not work in this regime because it does not take into account the discreteness of the lattice. As the size of the invaded region increases, lattice effects become unimportant. We find that all curves have converged onto the universal scaling function g for $P \geq 0.4$. This gives one limit on the size of the critical scaling region.

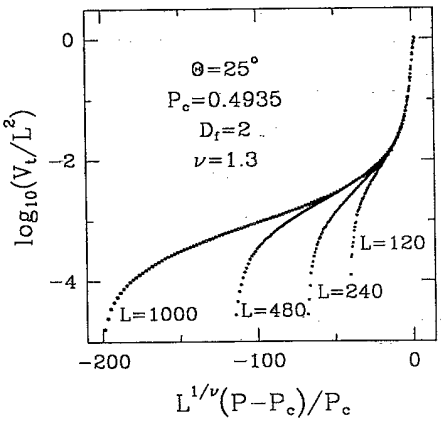

FIG. 6. Collapse of data from Fig. 5 onto a universal curve obeying Eq. (8). Values of the exponents are given and L ranges from 120 to 1000.

Another limit is provided by the range of pressures over which the density of instabilities (dy/dP) is approximately constant. Variations in dy/dP clearly modify the ratio between χ and $\langle V \rangle$ in Eq. (13). They also add additional pressure dependence to the scaling of other quantities. We find that dy/dP is nearly constant for $P \geq 0.4$, but changes rapidly at lower pressures. Hence this condition gives the same limit for the scaling regime: $P > 0.4$. We will restrict the data plotted in most subsequent figures to the scaling region.

Results for nonwetting invasion ($\theta = 179°$) were analyzed in a similar manner. In Fig. 7 we show plots of V_t/L^{D_f} versus $L^{1/\nu}(P - P_c)/P_c$ for $P_c = 5.62$, $D_f = \frac{91}{48} \approx 1.896$, and $\nu = \frac{4}{3}$. These values of D_f and ν equal those for ordinary 2D percolation, and provide a good collapse of the data. As above, bounds on D_f were obtained by examining plots of V_t/L^{D_f} versus P and requiring that all curves have a common intersection. This gave $D_f = 1.88 \pm 0.04$, which is consistent with results obtained by direct analysis of the invaded patterns.[36] The calculated[6,36] fractal dimension of the external interfaces of these patterns was $D_e = 1.32 \pm 0.02$.

Similar scaling fits were obtained for the total interfacial area. For wetting invasion, the results were consistent with $\omega = 0$ — the value of S_e saturated as P increased. For nonwetting invasion, the total interfacial area diverged. Data from all system sizes were collapsed onto a single curve using the value of ω obtained from exact 2D percolation exponents (Table II). Values of ω below 0.37 or above 0.47 were clearly inconsistent with the data.

B. Mean growth size

The exponents describing the mean growth size were obtained in the same way as exponents for the total in-

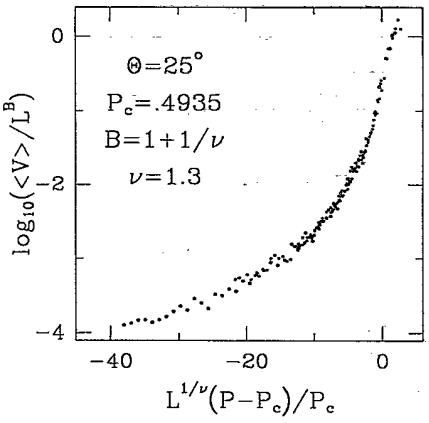

FIG. 8. Finite-size scaling collapse of data for $\langle V \rangle$ at $\theta = 25°$ [Eq. (14)]. Scaling parameters are indicated and L ranges from 120 to 1000.

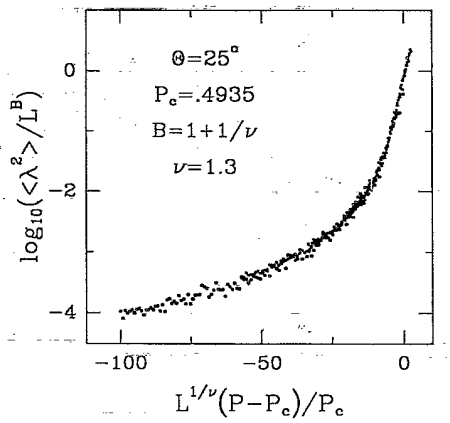

FIG. 10. Finite-size scaling collapse of data for $\langle \lambda^2 \rangle$ at 25° [Eq. (15)]. System sizes range from $L = 120$ to 1000 and values of scaling parameters are shown.

vaded volume. Values of B and P_c were determined by plotting $\langle V \rangle / L^B$ versus P and tuning B until all curves intersected at a common point, P_c [Eq. (14)]. For wetting invasion we found $B = 1.75 \pm 0.10$ and for nonwetting invasion $B = 1.30 \pm 0.10$. Results for P_c were the same as those found from the scaling of V_i (Table II).

Figures 8 and 9 show the universal curves implied by Eq. (14) for $\theta = 25°$ and 179°, respectively. The values of the scaling exponents and P_c are indicated. Note that the values of ν used to collapse data for V_i also collapse data for the mean growth size. As discussed further below, these values of ν and the values of B quoted above are consistent with the scaling relations of Table I.

C. Coherence length λ

As noted above, we find that $\langle \lambda^2 \rangle$ and $\langle V \rangle$ scale with the same exponent ϕ for $\theta < \theta_c$. This was tested by plotting the ratio $\langle \lambda^2 \rangle / \langle V \rangle$ in the scaling region below P_c. At $\theta = 25°$, the ratio is very constant until finite-size effects enter. The value of $\langle \lambda^2 \rangle$ is about seven times larger than $\langle V \rangle$, indicating that growth is anisotropic. Cascades of growth instabilities propagate more easily along the interface than perpendicular to it. Since $\langle \lambda^2 \rangle$ is larger than $\langle V \rangle$, finite-size effects become important at a slightly lower value of the scaling variable x.

Figure 10 shows a finite-size scaling collapse of data for $\langle \lambda^2 \rangle$ with system sizes ranging from $L = 120$ to 1000. The values of P_c, B, and ν are the same as those used

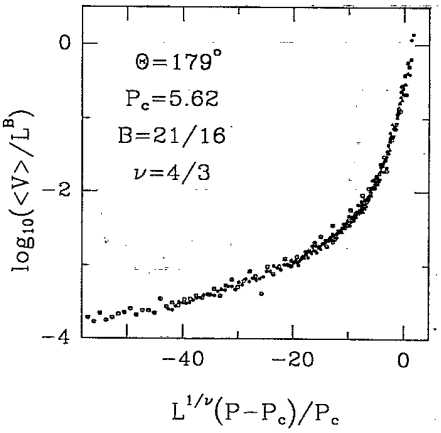

FIG. 9. Collapse of data for $\langle V \rangle$ at $\theta = 179°$ with L ranging from 60 to 600. Values of scaling parameters are shown.

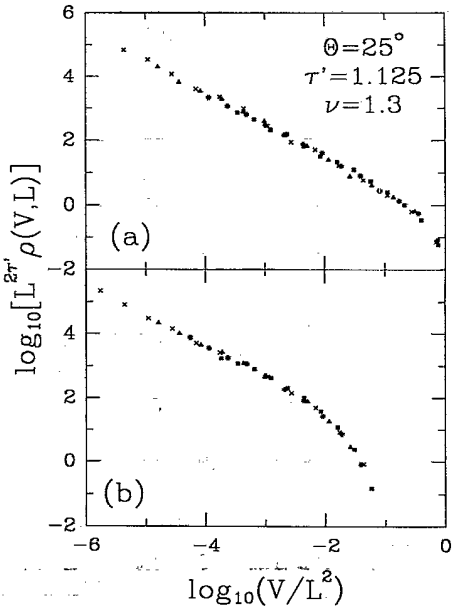

FIG. 11. Finite-size scaling collapse of results for $\rho(V, L)$ at $\theta = 25°$ for $L = 120, 240, 480$, and 1000. Growths were in a range of $L^{1/\nu}(P - P_c)/P_c$ from (a) -1 to 1 and (b) -5 to -3. The indicated scaling parameters were used for both panels.

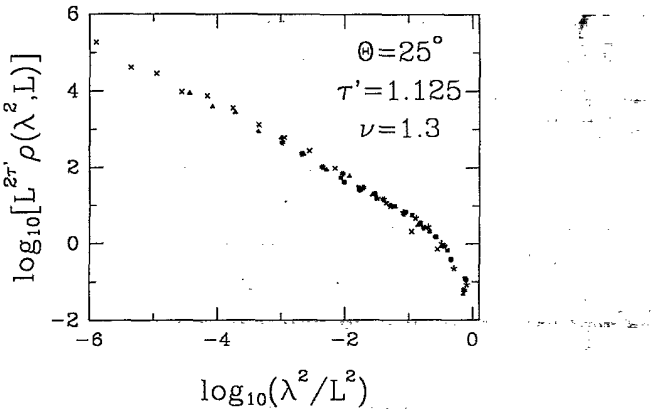

FIG. 12. Finite-size scaling collapse of results for $\rho(\lambda^2, L)$. Data were obtained at $\theta = 25°$ for $L = 120, 240, 480$, and 1000 and growths in the range $L^{1/\nu}|P - P_c|/P_c < 1$. Scaling parameters are indicated.

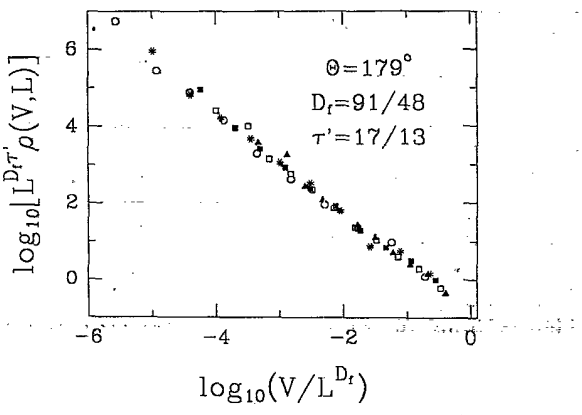

FIG. 13. Finite-size scaling of distribution of growths, $\rho(V, L)$, for $\theta = 179°$ and $L = 30, 60, 120, 300$, and 600. Data were taken from a range of $L^{1/\nu}(P - P_c)/P_c$ between -1 and $+1$. Scaling parameters are indicated.

for $\langle V \rangle$ in Fig. 8. The fit is very good, as expected from the proportionality noted above.

For nonwetting invasion, the value of $\langle \lambda^2 \rangle$ at P_c is finite and scales with the fingerwidth.[6] However, we find that $\bar{\lambda}$ diverges. The results satisfy Eq. (16) with $\bar{B} = 1.3 \pm 0.1$, and the same ν and P_c found for other scaling quantities. We confirmed that $\bar{B}$ was larger than B by verifying that the ratio $\langle \bar{\lambda}^2 \rangle / \langle V \rangle$ increased as $P \to P_c$. The increase was consistent with the difference between $\bar{B}$ and B calculated from ordinary percolation exponents (Table II).

D. Distributions of growths

We first consider the wetting case, $\theta = 25°$. Distributions for each L were averaged over the same range of the scaling parameter $L^{1/\nu}(P - P_c)/P_c$, so that ξ/L was the same. Figure 11(a) shows $\rho(V, L)$ for $L^{1/\nu}|P - P_c|/P_c < 1$. Here $\xi > L$ and the distribution is only cut off by the system size. As implied by Eq. (17), all results collapse onto a universal curve with $\tau' = 1.125 \pm 0.025$. Note that power-law scaling is observed over nearly 6 orders of magnitude in V. Figure 11(b) shows data from a pressure bin a little below P_c $[-5 < L^{1/\nu}(P - P_c)/P_c < -3]$. Here $\xi < L$, and the sharp downward bend for large volumes reflects the cutoff of growths larger than ξ^2.

Figure 12 shows the universal curve for the distribution of λ^2 when $L^{1/\nu}|P - P_c|/P_c < 1$ and $\tau' = 1.125$. The fit is excellent, demonstrating that the distributions of λ^2 and V have the same exponent. This is expected from the result that both scale with the same values of B and ν.

Figure 13 shows the scaled distribution of growths for nonwetting invasion ($\theta = 179°$) when $L^{1/\nu}|P - P_c| < 1$. Scaling is again observed over almost 6 orders of magnitude. For this angle we find $\tau' = 1.30 \pm 0.05$, which is slightly larger than the value for $\theta = 25°$.

The power-law distribution of volumes evident in Fig. 13 is related to the dynamic scaling behavior found in previous simulations of invasion percolation.[51] Since a single instability allows large connected regions to advance, there will be correlations in the invasion of nearby sites. The probability that sites invaded at times separated by t are a distance r apart obeys power-law scaling.[51] It should be possible to derive relations between the exponents describing this scaling and the exponents (Table I) describing the distribution of growth sizes and the fractal structure of the patterns.

E. Test of scaling laws

Table II summarizes our results for the critical exponents which describe wetting ($\theta = 25°$) and nonwetting ($\theta = 179°$) invasion. Exponents and error bars were obtained independently from separate fits for each quantity as described above. The quoted error bars indicate estimates of the maximum range that could be consistent with our data. They do not include systematic errors. Also included in Table II are exponents from standard 2D percolation. The exponents ψ, ϕ, B, and τ' have not been calculated previously. The quoted values were computed from the scaling relations in Table I.

All fitted exponents for nonwetting invasion are consistent with standard percolation values and with the scaling relations in Table I. For this reason we have used the exact percolation exponents to collapse data for $\theta = 179°$ in all of our figures. These exponents collapse data for several independent quantities with a single adjustable parameter P_c. Since the exponents ψ, ϕ, B, and τ' are new, agreement between fitted and calculated values constitutes a successful test of our scaling relations. Limited results for $\theta = 90°$ are consistent with the same exponents, indicating that they are universal.

Previous work[35] has indicated that the fractal dimension of invaded patterns is nonuniversal and may be smaller than that of a percolation cluster because of

trapped regions.[33] Although it is clear that trapping reduces the invaded volume, this does not necessarily reduce D_f. Trapping cannot change the external fractal dimension D_e, and should not affect ν. Inserting the smallest calculated value,[35,44] $D_f = 1.82$, into our scaling relations gives $\tau' = 1.32$ and $B = 1.30$. These values are within our error bars, but do not give as good a collapse of the data as the values used in Figs. 7, 9, and 13. Moreover, all of our direct determinations of D_f indicate that it is close to the usual percolation value.[6,36] Thus trapping does not appear to lower D_f in our growth model. It would be interesting to determine whether the exponents characterizing growth in the invasion percolation model are consistent with a smaller value of D_f.

The exponents obtained for wetting invasion (Table II) are also consistent with all scaling relations. For instance, the value of ν would imply $B = 1.77 \pm 0.06$, while τ' would give $B = 1.75 \pm 0.05$. Both values are in excellent agreement with the value obtained directly.

A single optimum set of exponents for wetting invasion was obtained by assuming that the scaling relations are valid and varying the single parameter ν to determine a best global fit. This gave $\nu = 1.30$. The resulting exponents were used in all finite-size scaling plots shown above. This single exponent fit collapses data for all quantities.

To test for universality in wetting invasion, data were obtained for $\theta = 40°$ and for different initial interfaces at 25° (inequivalent orientations and self-affine curves). All results were consistent with the same set of exponents used in the figures shown here. Thus it appears that the exponents for wetting invasion are also universal.

V. SUMMARY AND CONCLUSIONS

The results presented in the preceding section provide a detailed picture of the critical behavior of advancing interfaces in wetting and nonwetting invasion. The finite-size scaling ansatz and scaling relations developed in Sec. III allow data for all quantities and system sizes to be collapsed onto universal curves given ν, P_c, D_f, and D_e. Fitted values for D_f and D_e agree well with exact results for percolation and compact growth, and with values determined directly from analysis of the invaded patterns.

Wetting and nonwetting invasion belong to different universality classes. Nonwetting invasion is well described by critical exponents from ordinary percolation,[34] while the exponents for wetting invasion appear to be in a new universality class. One obvious difference is in the fractal dimensions of the invaded patterns, but structural differences affect other critical exponents as well. For example, the value of ϕ is smaller for nonwetting invasion because trapping and overhangs tend to limit growth (Fig. 3). Growths that start from a point in an area where the displaced fluid is nearly surrounded by the invading fluid are likely to hit a nearby section of the interface before they can advance appreciably. The influence of morphology is directly reflected in the scaling relations (Table I), which show that $\phi - 1$ is proportional to the difference between bulk and external dimensions.

The real world is three dimensional and it is interesting to ask how our results will change in higher dimensions. Nonwetting invasion should still be described by the invasion percolation model and percolation critical exponents. Studies of invasion percolation in 3D show that trapping is very unlikely and that the value of D_f equals that for ordinary percolation.[35] Wetting invasion has not been studied theoretically, but the higher connectivity in 3D should favor coherent growth and increase θ_c. Indeed, recent experiments in glass bead packs observe an increase in θ_c with the effective dimensionality of the medium.[52] Some insight into 3D fluid invasion may be provided by studies of the related problem of driven magnetic domain wall motion.[9] Work in progress indicates that motion is characteristic of percolation for strong disorder, and that there is a transition to compact growth with a self-affine interface as the disorder is weakened. Preliminary data[53] are consistent with the scaling relations of Table I.

Another important extension of the work reported here, would be to study the critical behavior for P greater than P_c where there is continuous flow. Much of the work on CDW conduction,[4,15–17] and some work on self-organized critical phenomena,[10,54] has focused on this regime. Dynamic exponents can be identified which describe the divergence of a coherence length as P decreases to P_c, or the relation between the excess pressure $P - P_c$ and the mean flow velocity. It would be interesting to establish the relation between these exponents and the exponents for $P < P_c$ listed in Table I. For example, by analogy with equilibrium critical phenomena, one might expect the exponent for the correlation length to be the same above and below P_c.

Note that percolation and compact invasion will exhibit very different behavior above P_c. The external interface of a compact pattern is confined and can advance in a steady manner. The external interface of a fractal pattern spans the entire system at P_c and can only advance by filling in disconnected regions. The behavior above P_c will depend on whether growth remains fractal or becomes compact at large length scales. If the growth remains fractal, the interfacial area increases continually and there is no steady-state flow velocity. This situation arises in invasion by a less viscous fluid, where viscous fingering produces large-scale fractal structure characteristic of diffusion limited aggregation.[3,26,55] If the invaded pattern becomes compact at large scales, the width of the interface and the mean flow rate will saturate at steady-state values. This situation arises when the invading fluid is *more* viscous[26] so that long-range viscous forces suppress fluctuations from a flat interface. In both cases the fractal structure found at P_c remains at short length scales, and the new scaling behavior begins above a crossover length. The crossover length must diverge as P decreases to P_c, and should correspond to the dynamic correlation length. The nonlocal nature of viscous effects makes it difficult to construct realistic models of fluid invasion, but simpler models of the dynamics may provide insight. Examples of such models are driven magnetic domain wall motion or related continuum equations, such as Eq. (1) with quenched disorder.

We briefly mention one example of a possible connec-

tion between invasion above and below P_c. The observed power-law spectrum of growths can naively be related to temporal fluctuations. If we assume a constant flow rate during invasion, the time T_V needed to invade a region of volume V is proportional to V. The distribution of invasion times scales simply as $\rho(T_V) \sim T^{-\tau'}$. This implies a power-law noise spectrum.

Power-law distributions of growths and noise are also characteristic of self-organized critical phenomena.[10] The major difference is the presence of quenched disorder in moving interface, CDW, and related systems. In SOC models, disorder is produced dynamically from the initial conditions, randomness in dropping grains, etc. An important open question is how the nature of the disorder affects the observed critical behavior.

Note added in proof. The relation between τ', D_f, D_e, and ν given at the bottom left of Table I has been derived previously from very different arguments by Gouyet.[56] We thank the author for bringing this work on invasion in a gravational field to our attention. A minor difference is in the quoted *numerical* values of τ'. Gouyet assumed $D_e = \frac{7}{4}$, which gives $\tau' \approx 1.53$. Our simulations[6,36] are clearly inconsistent with these values of D_e and τ', and recent work by Birovljev *et al.*[57] confirms that $D_e = \frac{4}{3}$ for invasion percolation.

ACKNOWLEDGMENTS

We thank H. Ji, B. Koiller, R. A. MacDonald, J. P. Stokes, and C. Tang for useful discussions. Support from National Science Foundation Grant No. DMR-8553271 and the Donors of the Petroleum Research Foundation, administered by the American Chemical Society is gratefully acknowledged and N. M. acknowledges support from the NIST and the ASEE.

*Current address: National Institute of Standards and Technology, 226/B348, Gaithersburg, Maryland 20899.

[1] D. Bensimon, L. P. Kadanoff, S. Liang, B. I. Shraiman, and C. Tang, Rev. Mod. Phys. **58**, 977 (1986).

[2] D. A. Kessler, J. Koplik, and H. Levine, Adv. Phys. **37**, 255 (1988).

[3] See, e.g., J. Feder, *Fractals* (Plenum, New York, 1988).

[4] D. S. Fisher, Phys. Rev. Lett. **50**, 1486 (1983); Phys. Rev. B **31**, 1396 (1985).

[5] A. T. Fiory, A. F. Hebard, and W. I. Glaberson, Phys. Rev. B **28**, 5075 (1983).

[6] N. Martys, M. Cieplak, and M. O. Robbins, Phys. Rev. Lett. **66**, 1058 (1991).

[7] J. P. Stokes, A. P. Kushnick, and M. O. Robbins, Phys. Rev. Lett. **60**, 1386 (1988).

[8] M. O. Robbins and J.-F. Joanny, Europhys. Lett. **3**, 729 (1987); J. P. Stokes, M. J. Higgins, A. P. Kushnick, S. Bhattacharya, and M. O. Robbins, Phys. Rev. Lett. **65**, 1885 (1990).

[9] H. Ji and M. O. Robbins, Phys. Rev. A **44**, 2538 (1991); H. Ji, B. Koiller, and M. O. Robbins (unpublished).

[10] P. Bak, C. Tang, and K. Wiesenfeld, Phys. Rev. Lett. **59**, 381 (1987); Phys. Rev. A **38**, 364 (1988); P. Bak and K. Chen, Sci. Am. **264**, 46 (1991).

[11] J. M. Carlson and J. S. Langer, Phys. Rev. Lett. **62**, 2632 (1989).

[12] P. Sibani and P. B. Littlewood, Phys. Rev. Lett. **64**, 1305 (1990).

[13] A. A. Middleton, Ph.D. thesis, Princeton University, 1990; A. A. Middleton and D. S. Fisher, Phys. Rev. Lett. **66**, 92 (1991); and (unpublished).

[14] R. Myers and J. P. Sethna (unpublished).

[15] M. O. Robbins, J. P. Stokes, and S. Bhattacharya, Phys. Rev. Lett. **55**, 2822 (1985).

[16] S. Bhattacharya, M. J. Higgins, and J. P. Stokes, Phys. Rev. Lett. **63**, 1503 (1989).

[17] S. Coppersmith, Phys. Rev. Lett. **65**, 1044 (1990).

[18] R. Bruinsma and G. Aeppli, Phys. Rev. Lett. **52**, 1547 (1984).

[19] J. Koplik and H. Levine, Phys. Rev. B **32**, 280 (1985).

[20] J. V. Maher, W. I. Goldburg, D. W. Pohl, and M. Lanz, Phys. Rev. Lett. **53**, 60 (1984); D. A. Andelman and J. F. Joanny, in *Physics of Finely Divided Matter*, edited by N. Boccara and McDonald (Springer-Verlag, Berlin, 1985), p. 361.

[21] J.-F. Joanny and P.-G. de Gennes, J. Chem. Phys. **81**, 552 (1984).

[22] M. Kardar, G. Parisi, and Y. Zhang, Phys. Rev. Lett. **64**, 543 (1990); E. Medina, T. Hwa, M. Kardar, and Y.-C. Zhang, Phys. Rev. A **39**, 3053 (1989).

[23] H. Yan, D. Kessler, and L. M. Sander, Phys. Rev. Lett. **64**, 926 (1990).

[24] J. Amar and F. Family, J. Phys. A **24**, L79 (1991).

[25] L. P. Kadanoff, S. R. Nagel, L. Wu, and S. Zhou, Phys. Rev. A **39**, 6524 (1989).

[26] R. Lenormand, C. Zarcone, and A. Zorr, J. Fluid Mech. **135**, 337 (1983); R. Lenormand and C. Zarcone, Phys. Rev. Lett. **54**, 2226 (1985).

[27] R. Lenormand and C. Zarcone, SPE-13264, in *Proceedings of the Fifty-Ninth Annual Technological Conference and Exhibition of the Society of Petroleum Engineers, Houston, Texas, 1984* (Society of Petroleum Engineers, Richardson, TX, 1984).

[28] E. Peters and D. Flock, Soc. Pet. Eng. J. **21**, 249 (1981).

[29] J. P. Stokes, D. A. Weitz, J. P. Gollub, A. Dougherty, M. O. Robbins, P. M. Chaikin, and H. M. Lindsay, Phys. Rev. Lett. **57**, 1718 (1986).

[30] M. A. Rubio, C. Edwards, A. Dougherty, and J. P. Gollub, Phys. Rev. Lett. **63**, 1685 (1989); **65**, 1389 (1990).

[31] V. K. Horváth, F. Family, and T. Vicsek, Phys. Rev. Lett. **65**, 1388 (1990); J. Phys. A **24**, L25 (1991).

[32] J. G. Amar and F. Family, Phys. Rev. Lett. **64**, 543 (1990).

[33] R. Lenormand and S. Bories, C. R. Acad. Sci. Ser. B **291**, 279 (1980); R. Chandler, J. Koplik, K. Lerman, and J. F. Willemsen, J. Fluid Mech. **119**, 249 (1982).

[34] See, for example, D. Stauffer, *Introduction to Percolation Theory* (Taylor and Francis, London, 1985).

[35] D. Wilkinson and J. F. Willemsen, J. Phys. A **16**, 3365 (1983).

[36] M. Cieplak and M. O. Robbins, Phys. Rev. Lett. **60**, 2042 (1988); Phys. Rev. B **41**, 11 508 (1990).

[37] A fluid interface intersects a solid at a contact angle θ (Fig.

2) determined by surface energies, see P. G. de Gennes, Rev. Mod. Phys. **57**, 827 (1985).

[38] R. L. Chuoke, P. van Meurs, and C. van der Poel, Trans. Am. Inst. Min. Metall. Pet. Eng. **216**, 188 (1959).

[39] G. Li and L. M. Sander, Phys. Rev. A **36**, 4551 (1987).

[40] Koplik and Levine attributed Γ to viscous stabilization which occurs when the invading fluid is more viscous. While viscous effects can smooth the interface, they act nonlocally. In particular, for nonwetting invasion there is still self-similar fractal structure (Refs. 3 and 26).

[41] We use the word "volume" for the size of the invaded region because we will develop equations for arbitrary dimension.

[42] The perimeter of the enclosed trapped regions is excluded from S_e, since this internal interface is not allowed to grow.

[43] In principle, growth might be anisotropic with different exponents describing the correlation length parallel and perpendicular to the interface. The largest exponent would then dominate the finite-size scaling, and a single parameter scaling like that used here might still describe growth.

[44] Wilkinson and Willemson (Ref. 35) found that trapping decreased D_f in 2D. The value of D_f was nonuniversal, ranging from 1.82 for square and honeycomb lattices to 1.88 for hexagonal lattices. The geometry of our model is closest to the honeycomb lattice, but careful checks of D_f reveal no significant deviation from the ordinary percolation value. It is unclear whether the difference between these results reflects nonuniversality or uncertainties in determining D_f.

[45] If the initial interface had a lower dimension, the scaling form for V_t would be unchanged, but the asymptotic form of g would not. For example, if growth is from a small d-dimensional sphere, then V_t is independent of L in the low-P regime. This requires $g(x) \sim |x|^{-\nu D_f}$ at large negative x. The typical scale of outward growth is of order ξ.

[46] In principle, some sites that would become unstable in the pressure range will be destabilized by a preceding growth. However, if one requires that ΔP is small enough that only a small fraction of the interface advances, such interactions will be negligible. We verified that this expression for N was satisfied numerically.

[47] N. Martys, Ph.D. thesis, Johns Hopkins University, 1990; N. Martys, M. O. Robbins, and M. Cieplak, in *Scaling in Disordered Materials: Fractal Structure and Dynamics*, edited by J. P. Stokes, M. O. Robbins, and T. A. Witten (Materials Research Society, Pittsburgh, 1990), p. 67.

[48] In general, $\langle \lambda^d \rangle$ might diverge with a different exponent than $\langle V \rangle$. However, a necessary condition for the interface to be self-affine is that the lateral growth is at least as great as the forward growth. This condition requires that the value of B in Eq. (15) must be greater than or equal to that in Eq. (13).

[49] The exponent τ' is related to, but different from, the exponent τ describing the cluster distribution in ordinary percolation.

[50] Other aspect ratios were studied and gave the same exponents.

[51] L. Furuberg, J. Feder, A. Aharony, and T. Jossang, Phys. Rev. Lett. **61**, 2117 (1988).

[52] A. P. Kushnick, J. P. Stokes, and M. O. Robbins (unpublished).

[53] H. Ji and M. O. Robbins (unpublished).

[54] C. Tang and P. Bak, Phys. Rev. Lett. **60**, 2347 (1988).

[55] L. Paterson, Phys. Rev. Lett. **52**, 1621 (1984).

[56] J. F. Gouyet, Physica A **168**, 581 (1990).

[57] A. Birovljev *et al.*, Phys. Rev. Lett. **67**, 584 (1991).